In-Plane Ferroelectric Tunneling Junction

Huitao Shen,[1] Junwei Liu,[2] Kai Chang,[3] and Liang Fu[1]

[1]*Department of Physics, Massachusetts Institute of Technology, Cambridge, Massachusetts 02139, USA*
[2]*Department of Physics, Hong Kong University of Science and Technology, Clear Water Bay, Hong Kong, China*
[3]*Max-Planck Institute of Microstructure Physics, Weinberg 2, 06120 Halle (Saale), Germany*

The ferroelectric material is one of the important platforms to realize non-volatile memories. So far, existing ferroelectric memory devices utilize out-of-plane polarization in ferroelectric thin films. In this paper, we propose a new type of random-access memory (RAM) based on ferroelectric thin films with the in-plane polarization called "in-plane ferroelectric tunneling junction". Apart from non-volatility, lower power usage and faster writing operation compared with traditional dynamic RAMs, our proposal has the advantage of non-destructive reading process, thus overcomes the write-after-read problem that widely exists in current ferroelectric RAMs, and faster reading operation. The recent discovered room-temperature ferroelectric IV-VI semiconductor thin films is a promising material platform to realize our proposal.

To meet the daily increasing demands of modern electronic devices, especially of portable devices, memories with low energy consumption and high performance are highly desired. The current commercial dynamic random-access memories (DRAM) are volatile, which consume a large amount of energy to refresh the stored data in order to prevent leakage from the capacitor. To reduce the energy consumption, a non-volatile memory might be the ultimate solution [1, 2].

The ferroelectric material has been proposed to be an ideal candidate for non-volatile memories due to its electric switchable bistable ground states since 1952 [3], and ferroelectricity based non-volatile memories have been developed rapidly in the past several decades [4, 5].

Depending on the readout mechanism, ferroelectric non-volatile memories can be roughly classified into two generations. The first generation of ferroelectric RAM (FeRAM) uses polarized charges in the ferroelectric capacitor to represent the data [6–8]. As a result, discharging the capacitor to measure the polarized charge destroys the stored data, and the capacitor needs to be recharged after the reading operation. Limited by the destructive reading process, the ferroelectric size effects [9, 10] and various practical issues such as fatigue [11] and imprint [12], the market of FeRAM remains relatively small.

To overcome the destructive readout problem, the second generation of ferroelectric tunneling junction (FTJ) is proposed to probe the ferroelectric polarization using the tunneling electroresistance effect [13–15]. The basic structure of the FTJ is a metal-ferroelectric-metal junction, where the tunneling barrier potential is determined by the out-of-plane polarization in the ferroelectric layer. In this way, the FTJ realizes bistable resistance states. The major challenge of realizing FTJ is to fabricate ultrathin ferroelectric films so that the tunneling current surpasses the threshold of peripheral amplifiers. The depolarization field induced by the out-of-plane polarization dramatically suppresses the ferroelectric critical temperature or even destroys the ferroelectricity when the films

are too thin [16–19].

In this work, we propose a new type of ferroelectric memory which we call "in-plane ferroelectric tunneling junction". Different from FeRAM or FTJ, which employs bistable states of out-of-plane ferroelectric polarization to represent "ON" and "OFF", our proposal is based on the in-plane polarization of ferroelectric thin films. Due to the insufficient screening in two dimensions (2D), the in-plane polarization could induce strong band bending around the edge. Depending on the polarization direction, the upward/downward band bending could be used to represent the ON/OFF state. By measuring the out-of-plane tunneling current through the ferroelectric thin films, the bending direction can be detected and hence the stored information is read non-destructively. Moreover, our design enjoys great tunability. By choosing proper layer sizes and the insulator layer band gap, the tunneling current and the ON/OFF current ratio can be tuned simultaneously. The recently discovered room-temperature IV-VI semiconductor thin films with robust in-plane polarization provide a promising material platform to realize our proposal [20].

The paper is organized as follows. We first introduce in-plane ferroelectric polarizations and the induced robust band bending. Then we demonstrate the device design and explain its reading and writing mechanism in detail. The demonstration is supported by the quantum mechanical tunneling current simulation. Finally, we discuss the advantage of our design over conventional ferroelectricity based memories.

In-plane polarization Ferroelectricity as a symmetry-breaking state is generally destabilized by the finite-size effect. The out-of-plane ferroelectric polarization is found in perovskite ultrathin films, in which imperfect charge screening, substrate strain and chemical bonding play important roles in stabilizing ferroelectricity [21–26]. As already mentioned in the introduction, the critical temperature of these perovskite ferroelectric materials decreases with the film thickness. Surprisingly, the recent discovered in-plane polarization in SnTe is enhanced instead of
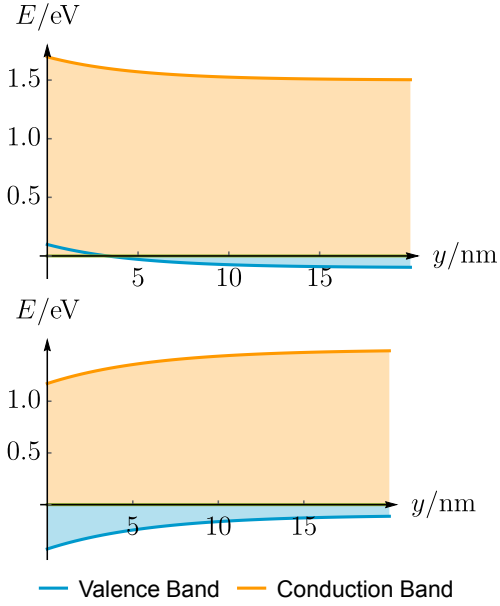
FIG. 1. Schematic of upward (top) and downward (bottom) band binding near the material edge. The parameters (band bending and band gap) are the same as measured in 1 ML SnTe [20]. To be more concrete, the bending parameter is in Table. I. The band gap is $\Delta_{\mathrm{FE}} = 1.6\mathrm{eV}$. Fermi energy of the electrode is set to be $E = 0$. The chemical potential is set to be $\mu_{\mathrm{FE}} = -0.1\mathrm{eV}$.

TABLE I. Fitted band bending from STM measurements for SnTe thin films with 1 ML taken from Ref. [20]. Here the substrate is metallic graphene. Note that the fitting parameter c is not the conduction band minimum (CBM) but the energy of the quantum well state.

Upward			Downward		
a(V)	λ(nm)	c(V)	a(V)	λ(nm)	c(V)
0.198	4.85	1.57	-0.329	6.12	1.57

reduced in thin films [20]. Compared with the bulk ferroelectric transition temperature of 98K, the one monolayer (ML) thin film has a critical temperature of 270K, and thicker films with 3 ML show robust spontaneous polarization even at room temperature.

An important signature of the in-plane polarization is the band bending near the material edge. Without screening, the bound charges induced by the in-plane ferroelectric polarization $\sigma_b = \mathbf{P} \cdot \mathbf{n}$ are of opposite signs at the two boundaries, where $\mathbf{P}$ is the polarization vector and $\mathbf{n}$ is the normal vector of the boundary. The resulting electric field leads to a linear band tilting in 3D and a logarithmic one in 2D, where the energy decreases from the negatively charged boundary to the positively charged boundary. When free charge carriers are present, which could be contributed from the substrate or the defects in the ferroelectric material, the screening effect cancels the boundary charge so that only the band bending near
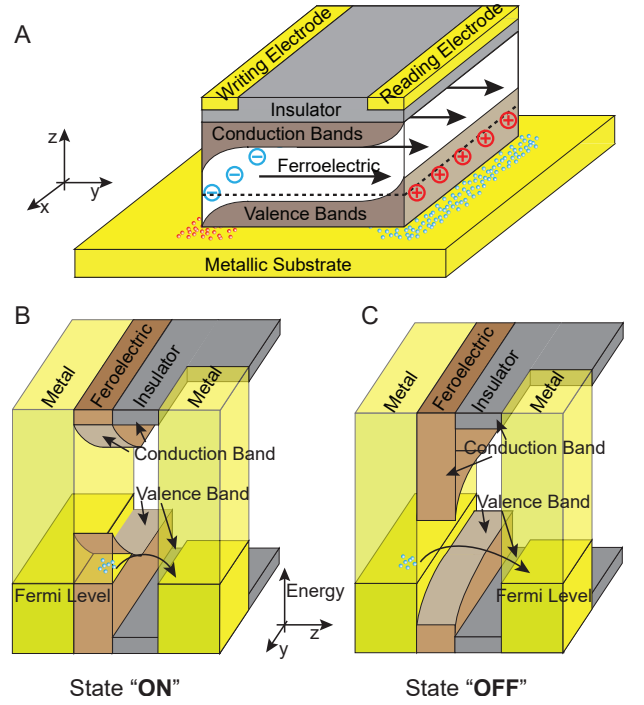

FIG. 2. Schematic of the device (A) and the band diagram of state "ON" (B) and "OFF" (C). The in-plane polarization induces bound charges and thus robust band bending around the boundary. Depending on the polarization direction, one of the edge could be conducting (B) or insulating (C), which will change the effective tunneling potential between the reading electrode and the substrate, therefore realizing bistable states with different tunneling currents. In panel (A), the large circles with "$+/-$" represent positive/negative bound charges induced by the ferroelectric polarization. The small red/blue dots represent positive/negative screening charges from the metallic substrate. The dashed line labels the Fermi level.

the boundary remains. In the following, we consider ferroelectric materials with large band gap so that the free charge carriers are from the metallic substrate. Due to the insufficient screening in 2D, the band bending can extend quite a region (several nanometers) near the boundary. For example, the scanning tunneling microscopy (STM) measured band bending near the boundary of 1 ML SnTe film can be fitted nicely by an exponential function $V = ae^{-x/\lambda} + c$, with parameters shown in Table I. SnTe thin films with odd number of monolayers all share similar band bending profile. We emphasize that this band bending near the boundary generally exists for all ferroelectric thin films with in-plane polarization and does not depend crucially on material details.

Device Design The robust band bending induced by the in-plane polarization motivates us to propose a new type of non-volatile memory. The schematic of the device is shown in Fig. 2A. The core of the design is a ferroelectric thin film sandwiched by a metallic substrate and a wide-band-gap insulator. The writing electrode and the
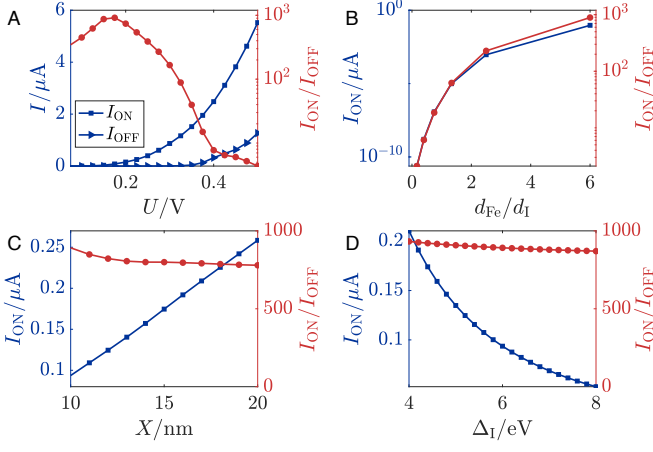
FIG. 3. Tunneling current computed from Landauer's formula Eq. (1) as function of different parameters. $X = Y = 10$nm, $d_{FE} = 6$nm, $d_I = 1$nm and $U = 0.18$V if not specified. Note that 1 ML SnTe is about 0.6nm thick [20] and monolayer h-BN is about 1.7nm thick [27]. (A) Bias voltage U; (B) Ferroelectric/insulator thickness ratio d_{FE}/d_I (total thickness fixed to be $Z = 7$nm); (C) Device width X; (D) Insulator band gap Δ_I. Chemical potential is always in the middle of the gap $\mu_I = -\Delta_I$.

reading electrode are deposited at two different edges of the top insulator that is (mostly) parallel to the polarization direction. In the figure, the in-plane polarization is assumed to be along the $+y$ direction, which will induce opposite net charges at different boundaries. Depending on the polarization direction ($+y$ or $-y$), the band bending near the reading electrode could be upward or downward, as is already discussed in the previous paragraph. The band diagram near one of the electrode is shown in Fig. 2B and Fig. 2C.

To write the information or manipulate the polarization direction, one can apply a writing voltage $\pm V_W$ on the writing electrode with reference to the reading electrode to generate an in-plane electric field across the ferroelectric thin film, thus forcing the polarization along $\pm y$ direction regardless of the initial polarization direction. The stored information is represented by the $\pm y$ polarization direction, which can be seen as the "0/1" bit. The polarization persists a longer duration even after the write voltage is turned off, and in this way the information storage is non-volatile. The time cost of the writing operation is determined by the polarization switching time, which in turn is determined by the applied writing voltage V_W. For example, the coercive field in GeTe thin films is reported to be $E_c = 0.206$V/nm, which translates to around $V_c = 20.6$V for writing and reading electrodes separated by 100nm [28]. For $V_W < V_c$, which is usually the case in a realistic device, the switching time is determined by the domain wall dynamics, which is typically several hundreds of picoseconds [29–31].

To read the information or measure the polarization

direction, one can apply a reading voltage V_R on the reading electrode with reference to the metallic substrate and measure the tunneling current. The tunneling current depends on the band bending and hence the polarization direction. More specifically, the tunneling current in the ON state I_{ON}, where the band bends upward near the reading electrode, is significantly larger than that in the OFF state I_{OFF}, where the band bends downward. Since the electric field generated by the reading voltage is perpendicular to the polarization, the reading process is non-destructive. Note that no capacitor discharge is involved in this process, the time cost of the reading operation is almost only determined by the peripheral current measurement device.

Tunneling Current We now turn to a detailed study of the tunneling electroresistance effect between the metallic substrate and the reading electrode. Without loss of generality, we assume the Fermi level of the metal is close to the valence band of the ferroelectric film. If the band bending is upward and strong enough, the valence band edge would be higher than the Fermi level of the metal, making the ferroelectric thin film conducting. In this case (ON state), the tunneling happens between the ferroelectric thin film and the reading electrode (Fig. 2B). It is worth noting that the above discussion also works for the scenario of downward band bending if the Fermi level in the metal is close to the conduction band of the ferroelectric film. On the other hand (OFF state), the downward band bending makes the ferroelectric thin film insulating. The tunneling then happens between the metallic substrate and the reading electrode (Fig. 2C). In this way, the threshold voltage for the ON state is determined by the band gap and the thickness of the insulator; while the ON/OFF ratio I_{ON}/I_{OFF} is determined by the band bending and the thickness of the ferroelectric thin film.

To make the above intuitive argument more concrete, we compute the tunneling current in a metal-ferroelectric-insulator-metal junction using two-terminal Landauer's formula

$$I = \frac{2e}{h} \int_{-\infty}^{\infty} T(E) \left[f_L(E) - f_R(E) \right] dE = \frac{2e}{h} \int_0^U T(E) dE, \tag{1}$$

where $T(E)$ is the transmission probability and $f_{L/R}(E) = \left[e^{-(E - \mu_{L/R})/k_B T} + 1 \right]^{-1}$ is the Fermi-Dirac distribution function. μ_L and μ_R are the chemical potential of the left and the right electrode respectively. In the following, we always set $\mu_L = 0$ as the reference. At zero temperature, $f_{L/R}(E)$ becomes the step function and Eq. (1) reduces to its final form, where $U \equiv \mu_R - \mu_L$ is the voltage bias.

The geometry of the system is taken to be the same as the device design in Fig. 2, where from the $-z$ to $+z$ there are in order: the left metal electrode (substrate), the ferroelectric, the insulator, the right metal electrode (reading electrode). The dimension is $X \times Y \times Z$. Here

$Z = d_{\text{FE}} + d_{\text{I}}$, which is the thickness of the ferroelectric and the insulator film respectively.

Inside the junction, the electrons and the holes are governed by the Schrödinger equation

$$\left[-\frac{\hbar^2 \nabla^2}{2m^*} + V(x, y, z) \right] \psi = E\psi. \tag{2}$$

The potential of the ferroelectric $V(x, y, 0 \leq z < d_{\text{FE}})$ is modeled by the fitted potential of 1 ML SnTe thin film (Fig. 1 and Table. I). The potential of the insulator $V(x, y, d_{\text{FE}} \leq z < d_{\text{FE}} + d_{\text{I}})$ is modeled by a square potential of monolayer h-BN. The band gap of the ferroelectric film and the insulator is chosen to be $\Delta_{\text{FE}} = 1.6\text{eV}$ [20] and $\Delta_{\text{I}} = 6\text{eV}$ respectively [32]. The chemical potential of the ferroelectric and the insulator are set to be $\mu_{\text{FE}} = -0.1\text{eV}$ and $\mu_{\text{I}} = -\Delta_{\text{I}}/2 = -3\text{eV}$ respectively.

Due to the complicated shape of the potential, the transmission probability in Eq. (1) is computed numerically using Kwant package [33] based on the discretized version Eq. (2). Both tunneling current contributions from the electrons and the holes are taken into account. The calculation detail can be found in [34]. The results are summarized in Fig. 3. Since the magnitude of the tunneling current and the ON/OFF ratio are two quantities that determine the sensitivity and the accuracy of the peripheral current measuring device, we mostly focus on them. We emphasize that although we take parameters of SnTe thin film in our simulation, the qualitative conclusion is independent of the material.

We first focus on the voltage-current characteristic (Fig. 3A). When the reading voltage is very small, both the current of the ON state and the OFF state come from the tunneling. With increasing the voltage, there is first a threshold in the ON state, after which $V > V_{\text{ON}}$ and the Ohm's law $I \propto U$ governs. The threshold voltage of the OFF state V_{OFF} is larger than that of the ON state. In Fig. 3A, $V_{\text{ON}} \approx 0.1\text{V}$ and $V_{\text{OFF}} \approx 0.4\text{V}$. When the voltage is in between the two threshold voltages, i.e. $V_{\text{ON}} < V < V_{\text{OFF}}$, a very large ON/OFF ratio decreases exponentially with the voltage. In order to maximize the ON/OFF ratio, it is important for the bias voltage to be within this "sweet spot".

From a device design point of view, the ON/OFF ratio and the size of the "sweet spot" $V_{\text{OFF}}/V_{\text{ON}}$ can be enhanced by increasing the $d_{\text{FE}}/d_{\text{I}}$ ratio, as is shown in Fig. 3B. This can be understood from our intuitive argument before—The difference of the tunneling region between the ON state and the OFF state is the ferroelectric film. This result suggests that the thickness of the insulator film d_{I} should be small, but still large enough to prevent the electric discharge between the electrodes. Note that for fixed total thickness, increasing $d_{\text{FE}}/d_{\text{I}}$ also increases the magnitude of the ON state current significantly. The ON/OFF ratio can be as large as ~ 1000 for $d_{\text{FE}}/d_{\text{I}} = 6/1$.

The magnitude of the ON state current after the threshold $V > V_{\text{ON}}$ can be enhanced by simply increasing the width of the device in the x direction. As shown in Fig. 3C, I_{ON} increases linearly with X because the number of modes per unit energy in the electrode also grows linearly. It is also possible to increase the current magnitude by decreasing the band gap of the insulator layer Δ_{I} (Fig. 3D). Note that for both approaches, the ON/OFF ratio is almost unaffected, implying an independent control of the ON state current and the ON/OFF ratio.

Conclusion In conclusion, we have proposed a new type of ferroelectric memory based on the in-plane polarization. Compared with the DRAM or the out-of-plane polarization based FeRAM, our design has advantages including non-volatility, non-destructive reading operation, faster reading and writing operation, and the greater tunability of the tunneling current and the ON/OFF ratio. Our design is based on the ferroelectric thin film with in-plane polarization component that is switchable by an external electric field. Compared with FTJ, the in-plane polarization is much more robust in thin films. A wide family of materials, for example, the IV-VI semiconductors XY [35–37], where X=Ge,Sn,Pb and Y=S,Se,Te, along with their alloys (for example, $Pb_xSn_{1-x}Se$) and superlattices (for example, PbTe/SnTe), are ideal candidates to realize our proposal. We hope our design can open up a new direction of ferroelectric non-volatile memories.

---

[1] J F Scott, "Multiferroic memories," Nat. Mater. **6**, 256 (2007).

[2] Kinam Kim and Dong Jin Jung, "Future Memory Technology and Ferroelectric Memory as an Ultimate Memory Solution," in *Ferroelectrics*, edited by Mickal Lallart (InTech, Rijeka, 2011) Chap. 6.

[3] Dudley Allen Buck, *Ferroelectrics for Digital Information Storage and Switching*, Tech. Rep. (Massachusetts Institute of Technology, 1952).

[4] James F. Scott and Carlos A. Paz de Araujo, "Ferroelectric memories," Science **246**, 1400–1405 (1989).

[5] James F Scott, *Ferroelectric Memories*, Vol. 3 (Springer-Verlag Berlin Heidelberg, 2013).

[6] J. T. Evans and R. Womack, "An experimental 512-bit nonvolatile memory with ferroelectric storage cell," IEEE J. Solid-State Circuits **23**, 1171–1175 (1988).

[7] R. Womack and D. Tolsch, "A 16 kb ferroelectric nonvolatile memory with a bit parallel architecture," in *IEEE International Solid-State Circuits Conference, 1989 ISSCC. Digest of Technical Papers* (1989) pp. 242–243.

[8] Hiroshi Ishiwara, Masanori Okuyama, and Yoshihiro Arimoto, *Ferroelectric Random Access Memories*, Vol. 93 (Springer-Verlag Berlin Heidelberg, 2004).

[9] Shaoping Li, J.A. Eastman, Z. Li, C.M. Foster, R.E. Newnham, and L.E. Cross, "Size effects in nanostructured ferroelectrics," Phys. Lett. A **212**, 341–346 (1996).

[10] Céline Lichtensteiger, Matthew Dawber, and Jean-Marc Triscone, "Ferroelectric size effects," in *Physics of Ferroelectrics: A Modern Perspective* (Springer Berlin Heidelberg, 2007) pp. 305–338.

[11] A K Tagantsev, I Stolichnov, E L Colla, and N Setter, "Polarization fatigue in ferroelectric films: Basic experimental findings, phenomenological scenarios, and microscopic features," J. Appl. Phys. **90**, 1387–1402 (2001).

[12] B S Kang, Jong-Gul Yoon, D J Kim, T W Noh, T K Song, Y K Lee, J K Lee, and Y S Park, "Mechanisms for retention loss in ferroelectric Pt/Pb(Zr0.4Ti0.6)O3/Pt capacitors," Appl. Phys. Lett. **82**, 2124–2126 (2003).

[13] M. Ye. Zhuravlev, R. F. Sabirianov, S. S. Jaswal, and E. Y. Tsymbal, "Giant Electroresistance in Ferroelectric Tunnel Junctions," Phys. Rev. Lett. **94**, 246802 (2005).

[14] H. Kohlstedt, N. A. Pertsev, J. Rodríguez Contreras, and R. Waser, "Theoretical current-voltage characteristics of ferroelectric tunnel junctions," Phys. Rev. B **72**, 125341 (2005).

[15] Evgeny Y. Tsymbal and Hermann Kohlstedt, "Tunneling Across a Ferroelectric," Science **313**, 181–183 (2006).

[16] Dillon D. Fong, G. Brian Stephenson, Stephen K. Streiffer, Jeffrey A. Eastman, Orlando Auciello, Paul H. Fuoss, and Carol Thompson, "Ferroelectricity in Ultrathin Perovskite Films," Science **304**, 1650–1653 (2004).

[17] D. D. Fong, A. M. Kolpak, J. A. Eastman, S. K. Streiffer, P. H. Fuoss, G. B. Stephenson, Carol Thompson, D. M. Kim, K. J. Choi, C. B. Eom, I. Grinberg, and A. M. Rappe, "Stabilization of Monodomain Polarization in Ultrathin $PbTiO_3$ Films," Phys. Rev. Lett. **96**, 127601 (2006).

[18] D. A. Tenne, P. Turner, J. D. Schmidt, M. Biegalski, Y. L. Li, L. Q. Chen, A. Soukiassian, S. Trolier-McKinstry, D. G. Schlom, X. X. Xi, D. D. Fong, P. H. Fuoss, J. A. Eastman, G. B. Stephenson, C. Thompson, and S. K. Streiffer, "Ferroelectricity in Ultrathin $BaTiO_3$ Films: Probing the Size Effect by Ultraviolet Raman Spectroscopy," Phys. Rev. Lett. **103**, 177601 (2009).

[19] Emad Almahmoud, Igor Kornev, and L. Bellaiche, "Dependence of Curie temperature on the thickness of an ultrathin ferroelectric film," Phys. Rev. B **81**, 064105 (2010).

[20] K. Chang, J. Liu, H. Lin, N. Wang, K. Zhao, Anmin Zhang, Feng Jin, Yong Zhong, Xiaopeng Hu, Wenhui Duan, Q. Zhang, L. Fu, Q.-K. Xue, X. Chen, and S.-H. Ji, "Discovery of robust in-plane ferroelectricity in atomic-thick SnTe," Science **353**, 274–278 (2016).

[21] R. R. Mehta, B. D. Silverman, and J. T. Jacobs, "Depolarization fields in thin ferroelectric films," J. Appl. Phys **44**, 3379–3385 (1973).

[22] Javier Junquera and Philippe Ghosez, "Critical thickness for ferroelectricity in perovskite ultrathin films," Nature **422**, 506 (2003).

[23] Zhongqing Wu, Ningdong Huang, Zhirong Liu, Jian Wu, Wenhui Duan, Bing-Lin Gu, and Xiao-Wen Zhang, "Ferroelectricity in $Pb(Zr_{0.5}Ti_{0.5})O_3$ thin films: Critical thickness and $180°$ stripe domains," Phys. Rev. B **70**, 104108 (2004).

[24] Na Sai, Alexie M. Kolpak, and Andrew M. Rappe, "Ferroelectricity in ultrathin perovskite films," Phys. Rev. B **72**, 020101 (2005).

[25] Na Sai, Craig J. Fennie, and Alexander A. Demkov, "Absence of Critical Thickness in an Ultrathin Improper Ferroelectric Film," Phys. Rev. Lett. **102**, 107601 (2009).

[26] Yajun Zhang, Gui-Ping Li, Takahiro Shimada, Jie Wang, and Takayuki Kitamura, "Disappearance of ferroelectric critical thickness in epitaxial ultrathin $BaZrO_3$ films," Phys. Rev. B **90**, 184107 (2014).

[27] Kun Ba, Wei Jiang, Jingxin Cheng, Jingxian Bao, Ningning Xuan, Yangye Sun, Bing Liu, Aozhen Xie, Shiwei Wu, and Zhengzong Sun, "Chemical and Bandgap Engineering in Monolayer Hexagonal Boron Nitride," Sci. Rep. **7**, 45584 (2017).

[28] Wenhui Wan, Chang Liu, Wende Xiao, and Yugui Yao, "Promising ferroelectricity in 2D group IV tellurides: a first-principles study," Appl. Phys. Lett **111**, 132904 (2017).

[29] Rolf Landauer, "Electrostatic Considerations in BaTiO3 Domain Formation during Polarization Reversal," J. Appl. Phys **28**, 227–234 (1957).

[30] J. Li, B. Nagaraj, H. Liang, W. Cao, Chi. H. Lee, and R. Ramesh, "Ultrafast polarization switching in thin-film ferroelectrics," Appl. Phys. Lett **84**, 1174–1176 (2004).

[31] Kenjiro Fujimoto and Yasuo Cho, "Nanosecond Switching of Nanoscale Ferroelectric Domains in Congruent Single-Crystal $LiTaO_3$ Using Scanning Nonlinear Dielectric Microscopy," Jpn. J. Appl. Phys **43**, 2818 (2004).

[32] Yoichi Kubota, Kenji Watanabe, Osamu Tsuda, and Takashi Taniguchi, "Deep Ultraviolet Light-Emitting Hexagonal Boron Nitride Synthesized at Atmospheric Pressure," Science **317**, 932–934 (2007).

[33] Christoph W Groth, Michael Wimmer, Anton R Akhmerov, and Xavier Waintal, "Kwant: a software package for quantum transport," New J. Phys **16**, 063065 (2014).

[34] See Supplemental Material for calculation details, which includes Ref. [38].

[35] Hua Wang and Xiaofeng Qian, "Two-dimensional multiferroics in monolayer group IV monochalcogenides," 2D Materials **4**, 015042 (2017).

[36] Menghao Wu and Xiao Cheng Zeng, "Intrinsic Ferroelasticity and/or Multiferroicity in Two-Dimensional Phosphorene and Phosphorene Analogues," Nano Lett. **16**, 3236–3241 (2016).

[37] Kai Liu, Jinlian Lu, Silvia Picozzi, Laurent Bellaiche, and Hongjun Xiang, "Intrinsic origin of enhancement of ferroelectricity in snte ultrathin films," Phys. Rev. Lett. **121**, 027601 (2018).

[38] O. Madelung, U. Rössler, and M. Schulz, eds., "Tin telluride (SnTe) effective masses," in *Non-Tetrahedrally Bonded Elements and Binary Compounds I* (Springer Berlin Heidelberg, Berlin, Heidelberg, 1998) pp. 1–4.

Supplemental Material for "In-Plane Ferroelectric Tunneling Junction"

Huitao Shen,[1] Junwei Liu,[2] Kai Chang,[3] and Liang Fu[1]

[1] *Department of Physics, Massachusetts Institute of Technology, Cambridge, Massachusetts 02139, USA*
[2] *Department of Physics, Hong Kong University of Science and Technology, Clear Water Bay, Hong Kong, China*
[3] *Max-Planck Institute of Microstructure Physics, Weinberg 2, 06120 Halle (Saale), Germany*

In this Supplemental Material, we present the quantum transport simulation in detail.

As mentioned in the main text, we use two-terminal Landauer's formula to compute the tunneling current:

$$I = \frac{2e}{h} \int_{-\infty}^{\infty} T(E) \left[f_L(E) - f_R(E) \right] dE, \tag{1}$$

where $T(E)$ is the transmission probability and $f_{L/R}(E) = \left[e^{-(E-\mu_{L/R})/k_B T} + 1 \right]^{-1}$ is the Fermi-Dirac distribution function. μ_L and μ_R are the chemical potentials of the left and right electrode respectively. Here the factor of 2 is due to the spin degeneracy. In the following, we always set $\mu_L = 0$ as the reference. At zero temperature, $f_{L/R}(E)$ becomes the step function and Eq.(1) reduces to

$$I = \frac{2e}{h} \int_0^{\mu_R} T(E) dE = \frac{2e}{h} \int_0^{U} T(E) dE, \tag{2}$$

where $U \equiv \mu_R - \mu_L$ is the voltage bias.

Because of the complicated shape of the potential, we exploit the numerical method to compute the transmission probability, where we first discretize the Scrödinger equation. It is straightforward to show that the discretized version of

$$-\frac{\hbar^2}{2m^*} \left[\frac{\partial^2 \psi}{\partial x^2} + \frac{\partial^2 \psi}{\partial y^2} + \frac{\partial^2 \psi}{\partial z^2} \right] + V(x, y, z)\psi = 0, \tag{3}$$

is

$$
(6t + V(x, y, z))\psi(x, y, z) - t \left[\psi(x + a, y, z) + \psi(x - a, y, z) + \right.
$$
$$
\left. \psi(x, y + a, z) + \psi(x, y - a, z) + \psi(x, y, z + a) + \psi(x, y, z - a) \right] = 0, \tag{4}
$$

where $t = \hbar^2/(2m^* a^2)$. a is the lattice constant in the discretized lattice and $a \to 0$ reduces Eq. (4) to (3). The discretization is a good approximation if $\lambda_F/a \gg 1$, where λ_F is the Fermi wavelength.

The geometry of the system is the shown in Fig. 1. The size of the reading electrode is $X \times Y$. The thickness of the ferroelectric film and the insulator film are d_{FE} and d_{I} respectively. The total thickness (electrodes not included) is defined as $Z \equiv d_{\text{FE}} + d_{\text{I}}$.
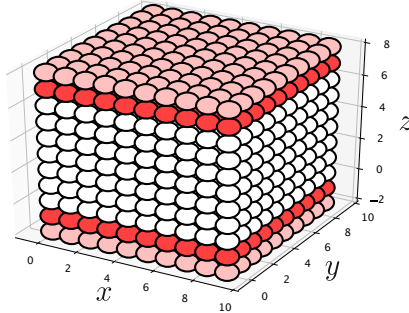

FIG. 1. Geometry of the system simulated in Kwant.

The tunneling potential of the ferroelectric film can be modeled by an exponential potential and that of the insulator can be modeled simply by a square potential. Here we have ignored the boundary effect at the interfaces of the electrode, the ferroelectric and the insulator. Both electrons and holes can contribute to the tunneling current. The effective potentials of these two tunneling channels are summarized in Table. I, which can be read from Fig. 1

in the main text. $\mu_{\text{FE}}/\Delta_{\text{FE}}$ and $\mu_{\text{I}}/\Delta_{\text{I}}$ are the chemical potential/band gap of the ferroelectric and the insulator respectively.

In the following, we use the parameter of thin SnTe film for the ferroelectric region and that of monolayer h-BN for the insulator region. The band gap of the ferroelectric film and the insulator is chosen to be $\Delta_{\text{FE}} = 1.6\text{eV}$ [1] and $\Delta_{\text{I}} = 6\text{eV}$ respectively [2]. The chemical potential of the ferroelectric and the insulator are set to be $\mu_{\text{FE}} = -0.1\text{eV}$ and $\mu_{\text{I}} = -\Delta_{\text{I}}/2 = -3\text{eV}$ respectively. Note that when $|\mu_{\text{FE}}| \ll |\Delta_{\text{FE}}|$, the current contribution are mainly from holes. The electrons are almost impossible to tunnel due to the high potential in the ferroelectric region.

TABLE I. Effective potentials for electrons and holes in different regions and states. Here we assume $\mu_{\text{FE}}, \mu_{\text{I}} < 0$ and $|\Delta_{\text{FE}}| > |\mu_{\text{FE}}|$, $|\Delta_{\text{I}}| > |\mu_{\text{I}}|$.

	Ferroelectric Region	Insulator Region
V_{h}	$\max\{-\alpha e^{-y/\lambda} - \mu_{\text{FE}}, 0\}$	$-\mu_{\text{I}}$
V_{e}	$\max\{\alpha e^{-y/\lambda} + \mu_{\text{FE}} + \Delta_{\text{FE}}, 0\}$	$\mu_{\text{I}} + \Delta_{\text{I}}$

For a typical semiconductor, m^*/m_e is usually between $0.01 - 0.1$ where m_e is the free electron mass and $\lambda_F \sim 1 - 10\text{nm}$. In the following calculation, we use parameters for SnTe $m^*/m_e = 0.1$ [3]. For the geometry, we choose $X = Y = 10\text{nm}$. d_{FE} and d_{I} are variables that are to be tuned. Note that 1 ML SnTe is about 0.6nm thick [1] and monolayer h-BN is about 1.7nm thick [4]. In the simulation, we take $a = 1\text{nm}$ [5].

[1] K. Chang, J. Liu, H. Lin, N. Wang, K. Zhao, Anmin Zhang, Feng Jin, Yong Zhong, Xiaopeng Hu, Wenhui Duan, Q. Zhang, L. Fu, Q.-K. Xue, X. Chen, and S.-H. Ji, "Discovery of robust in-plane ferroelectricity in atomic-thick SnTe," Science **353**, 274–278 (2016).

[2] Yoichi Kubota, Kenji Watanabe, Osamu Tsuda, and Takashi Taniguchi, "Deep Ultraviolet Light-Emitting Hexagonal Boron Nitride Synthesized at Atmospheric Pressure," Science **317**, 932–934 (2007).

[3] O. Madelung, U. Rössler, and M. Schulz, eds., "Tin telluride (SnTe) effective masses," in *Non-Tetrahedrally Bonded Elements and Binary Compounds I* (Springer Berlin Heidelberg, Berlin, Heidelberg, 1998) pp. 1–4.

[4] Kun Ba, Wei Jiang, Jingxin Cheng, Jingxian Bao, Ningning Xuan, Yangye Sun, Bing Liu, Aozhen Xie, Shiwei Wu, and Zhengzong Sun, "Chemical and Bandgap Engineering in Monolayer Hexagonal Boron Nitride," Sci. Rep. **7**, 45584 (2017).

[5] A technical note: In the calculation, we set $t = 1$ for convenience, so that the energy unit is

$$E_0 = \frac{\hbar^2}{2m^* a^2} \sim \frac{1}{m^*/m_e (a/a_0)^2} \times 13.6\,\text{eV}, \tag{5}$$

where a_0 is the Bohr radius. For the choice of $m^*/m_e = 0.1$ and $a = 1\text{nm}$, we have $E_0 = 0.38\text{eV}$. The current computed in Eq. (1) is in the unit of $29.5\mu\text{A}$.